

# **Measuring general relativistic dragging effects in the Earth's gravitational field with ELXIS: a proposal**

Lorenzo Iorio<sup>1</sup>

Ministero dell'Istruzione, dell'Università e della Ricerca (M.I.U.R.)-Istruzione  
Permanent address for correspondence: Viale Unità di Italia 68, 70125, Bari (BA), Italy

`lorenzo.iorio@libero.it`

Received \_\_\_\_\_; accepted \_\_\_\_\_

## Abstract

In a geocentric kinematically rotating ecliptical coordinate system in geodesic motion through the deformed spacetime of the Sun, both the node  $\Omega$  and the inclination  $I$  of an artificial satellite of the spinning Earth are affected by the post-Newtonian gravitoelectric De Sitter and gravitomagnetic Lense-Thirring effects. By choosing a circular orbit with  $I = \Omega = 90$  deg for a potential new spacecraft, which we propose to name ELXIS, it would be possible to measure each of the gravitomagnetic precessions separately at a percent level, or, perhaps, even better depending on the level of accuracy of the current and future global ocean tide models since the competing classical long-term perturbations on  $I$ ,  $\Omega$  due to the even and odd zonal harmonics  $J_\ell$ ,  $\ell = 2, 3, 4, \dots$  of the geopotential vanish. Moreover, a suitable linear combination of  $I$ ,  $\Omega$  would be able to cancel out the solid and ocean tidal perturbations induced by the  $K_1$  tide and, at the same time, enforce the geodetic precessions yielding a secular trend of  $-8.3$  milliarcseconds per year, thus strengthening the goal of a  $\simeq 10^{-5}$  test of the De Sitter effect recently proposed in the literature in the case of an equatorial coordinate system. Relatively mild departures  $\Delta I = \Delta \Omega \simeq 0.01 - 0.1$  deg from the ideal orbital configuration with  $I = \Omega = 90$  deg are allowed. Present-day, uncontroversial levels of relative accuracy in testing the geodetic and the gravitomagnetic effects in the field of the Earth are  $9 \times 10^{-4}$  (Lunar Laser Ranging) and  $1.9 \times 10^{-1}$  (Gravity Probe B), respectively.

keywords Experimental studies of gravity; Experimental tests of gravitational theories; Satellite orbits; Harmonics of the gravity potential field

## 1. Introduction

Iorio (2018) recently proposed to use a hypothetical new terrestrial artificial satellite, here dubbed<sup>1</sup> ELXIS and to be placed in a circular path in an orbital plane displaced by  $\Omega_{\text{eq}} = 90$  deg with respect to the reference direction of the Vernal Equinox  $\Upsilon$  perpendicularly to the Earth’s equator, in order to measure the general relativistic De Sitter effect (de Sitter 1916; Schouten 1918; Fokker 1920) on the orbital inclination  $I_{\text{eq}}$  to the equator (Iorio 2018) with a possible relative accuracy level of  $\simeq 10^{-5}$ . A rather strict polar orbital configuration, with departures as little as  $\Delta I_{\text{eq}} \simeq 10^{-3} - 10^{-5}$  deg, would be required to reduce the impact of the aliasing perturbations due to the solid and ocean components of the  $K_1$  tide, which would be one of the major sources of systematic errors, especially if not too high altitudes were to be adopted. The long-term rates of change of  $I_{\text{eq}}$  due to the even and odd zonal harmonics of the geopotential vanish for the orbital geometry proposed. It was tacitly assumed that the data analysis would be performed in

---

<sup>1</sup>From  $\xi\lambda\xi\iota\varsigma$ , which means ‘dragging’, ‘trailing’.

a geocentric kinematically rotating and dynamically non-rotating (Brumberg & Kopeikin 1989) coordinate system having the mean Earth’s equator at the reference epoch J2000.0 as reference  $\{x, y\}$  plane, and all the angular orbital elements in Iorio (2018) are to be intended as referred to it. Here, we recall that a coordinate system  $\mathcal{K}$  is said to be “dynamically non-rotating” if no fictitious forces like the Coriolis force, etc. affect the motion of a test particle referred to it (Brumberg & Kopeikin 1989). Furthermore, it is said to be “kinematically non-rotating” if it keeps the orientation of its reference directions, determined, e.g., by the axes of three mutually orthogonal spinning gyroscopes, with respect to distant quasars in its motion through the external gravitational field of a distant massive body, rotating or not, like, e.g., the Sun (Brumberg & Kopeikin 1989). A kinematically non-rotating coordinate system  $\mathcal{K}$  is not suitable for detecting the gravitoelectric<sup>2</sup> De Sitter effect (along with the gravitomagnetic Pugh-Schiff effect (Pugh 1959; Schiff 1960) if the source of the external gravitational field is rotating itself) since the latter one is nothing but that the reflex on the local motion of the axis of a gyroscope  $\xi$  as referred to  $\mathcal{K}$  itself of the change of the reference directions of  $\mathcal{K}$  due to its motion through the deformed spacetime of the external body assumed static. In other words, in a kinematically non-rotating coordinate system  $\mathcal{K}$ , the De Sitter precession is automatically corrected for, so that it does not show up in the motion of a gyroscope  $\xi$  whose center of mass is located at the origin of  $\mathcal{K}$  itself. In the present case,  $\xi$  has to be meant as the whole geocentric satellite’s orbit. In the usual data reductions, a kinematically non-rotating and dynamically rotating<sup>3</sup> geocentric equatorial coordinate system, the International Celestial Reference System (ICRS), is routinely used, i.e. the De Sitter precession is accounted for.

In this paper, we show that, by using a<sup>4</sup> kinematically rotating geocentric coordinate system with the mean ecliptic at J2000.0 as reference  $\{x, y\}$  plane, which preserves the same satellite’s orbital geometry of Iorio (2018), it is possible to suitably combine the (ecliptical) node  $\Omega$  and inclination  $I$ , both affected by the De Sitter precessions (Iorio 2018), in order to cancel out, by construction, the effect of both the solid and ocean perturbations due to the  $K_1$  tide and produce an overall De Sitter secular trend of about  $-8.3 \text{ mas yr}^{-1}$ . Such a combination would be impacted neither by the zonal 055.565 tide nor by the zonals of the geopotential whose perturbations on  $I$  and  $\Omega$  vanish for  $I = \Omega = 0 \text{ deg}$ , thus enforcing the goal of reaching a  $\simeq 10^{-5}$  level. Furthermore, it would also be possible to analyze the node and the inclination separately to measure the general relativistic Lense-Thirring effect (Lense & Thirring 1918) affecting each of them (Iorio 2011) to a few percent accuracy, or, in perspective, even better, depending on the accuracy of the present and

---

<sup>2</sup>The denominations “gravitoelectric” and “gravitomagnetic” for such general relativistic effects were introduced by Thorne (1983).

<sup>3</sup>It is so because of the fictitious forces in the satellite’s equations of motion arising from the rotation required to compensate the kinematic De Sitter precession with respect to distant quasars. They are included in the data processing algorithms in accordance with the IERS Standards (Petit, Luzum & et al. 2010).

<sup>4</sup>Here and in the following, it is assumed that it is also dynamically non-rotating.

future global ocean tide models adopted. The approach proposed in the present paper would allow to somewhat relax the strict conditions on  $I$ ,  $\Omega$  also for relatively low orbits with respect to Iorio (2018).

In assessing the level of accuracy obtainable with the presently proposed scenario, it should be kept in mind that, while the geodetic precession is currently known at the level of  $9 \times 10^{-4}$  (Hofmann & Müller 2018) from the Lunar Laser Ranging (LLR) technique, the only uncontroversial test of the gravitomagnetic field of the Earth published so far in the literature is the one performed with the past Gravity Probe B (GP-B) mission which reached an overall accuracy of 19% (Everitt et al. 2011, 2015).

The paper is organized as follows. In Section 2, a general scheme for obtaining the rates of change of the satellite’s inclination and node in the ecliptical coordinate system from the equatorial one is outlined. In Section 3, the long-term effects on  $I$ ,  $\Omega$  due to the general relativistic Lense-Thirring effect (Section 3.1) and the odd and even zonal harmonics  $J_\ell$ ,  $\ell = 2, 3, 4, \dots$  of the Earth’s geopotential (Section 3.2) are analytically and numerically worked out. It is shown that departures of  $\simeq 0.01 - 0.1$  deg from the ideal condition  $I = \Omega = 90$  deg would affect the mismodelled classical precessions to less than the percent level of the gravitomagnetic ones even by assuming very conservative uncertainties in the zonals themselves. Section 4 is devoted to the tidal perturbations induced on  $I$ ,  $\Omega$  by the solid (Section 4.1) and ocean (Section 4.2) components of the  $K_1$  tide for  $\ell = 2$ ,  $m = 1$ ,  $p = 1$ ,  $q = 0$  and their sensitivity to departures of the actual satellite’s inclination and nodes from the nominal scenario  $I = \Omega = 90$  deg (Section 4.3). It is shown that the largest nominal perturbations arise from the ocean tide; depending on the accuracy of the latest global ocean tide models, their impact on the Lense-Thirring rates may be as low as a few percent. A linear combination of the precessions of  $I$ ,  $\Omega$  able to cancel out the  $K_1$  tidal perturbations is designed (Section 4.4). Unfortunately, it would remove also the Lense-Thirring rates as well. In Section 5, it is shown that, instead, the De Sitter precessions are not canceled out by the aforementioned linear combination. The impact of the 3rd-body perturbations due to a distant perturber such as the Moon on both the individual precessions of the inclination and the node and their linear combination is treated in Section 6. In view of the present-day level of mismodeling in the lunar gravitational parameter, it turns out that the combined De Sitter trend would be affected, at most, at the  $\simeq 3 \times 10^{-5} - 1 \times 10^{-4}$  level, while the bias on the Lense-Thirring precessions taken individually would be negligible. A cursory overview of the impact of the non-gravitational perturbations on both the individual Lense-Thirring precessions and the combined De Sitter effect is given in Section 7. By relying upon Sec. (6) of Iorio (2018) for the inclination and on several works by other researchers for the node, it turns out that, for a geodetic satellite of LAGEOS-type, their effect can be deemed as negligible with respect to the accuracy goal in the proposed relativistic tests. In Section 8, we offer a comparison with the past proposal by van Patten & Everitt (1976b) encompassing the launch of two drag-free counter-orbiting spacecraft in nearly identical circular polar orbits. Our findings and conclusions are resumed in Section 9. Appendix A displays a list of definitions of all the physical and orbital parameters used in the text, while Appendix B contains the numerical values of most of them

along with the figures.

## 2. The rates of change of the inclination and the node in the ecliptic coordinate system

Basically, all the literature on some of the satellite orbital perturbations is developed in an equatorial coordinate system; thus, we need to devise a strategy to convert the existing analytical formulas for the equatorial rates of change of the satellite's orbital elements into expressions valid for the ecliptical coordinate system adopted here. Such an approach will turn out to be quite useful for gaining valuable information about, e.g., the tidal perturbations (see Section 4).

To this aim, let us start by rotating the normal unit vector  $\hat{n}$ , written in terms of the ecliptical elements, from the ecliptical to the equatorial system: the result is

$$\hat{n}^{\text{eq}} = \{\sin I \sin \Omega, -\cos \epsilon \cos \Omega \sin I - \cos I \sin \epsilon, \cos I \cos \epsilon - \cos \Omega \sin I \sin \epsilon\}. \quad (1)$$

Then, let us calculate the node and the inclination referred to the equator from the components of Equation (1) as

$$I_{\text{eq}}(I, \Omega; \epsilon) = \arctan \left( \frac{\sqrt{(\hat{n}_x^{\text{eq}})^2 + (\hat{n}_y^{\text{eq}})^2}}{\hat{n}_z^{\text{eq}}} \right), \quad (2)$$

$$\Omega_{\text{eq}}(I, \Omega; \epsilon) = \arctan \left( \frac{\hat{n}_x^{\text{eq}}}{-\hat{n}_y^{\text{eq}}} \right). \quad (3)$$

From Equations (2) to (3) it turns out that  $I, \Omega = 90 \text{ deg}$  correspond just to  $I_{\text{eq}}, \Omega_{\text{eq}} = 90 \text{ deg}$ . By taking the time derivatives<sup>5</sup> of Equations (2) to (3), it is possible to obtain exact analytical expressions of the rates of change of  $I_{\text{eq}}, \Omega_{\text{eq}}$  expressed in terms of their ecliptical  $I, \Omega$  counterparts. They get simplified for  $I = \Omega = 90 \text{ deg}$  reducing to

$$\dot{I}_{\text{eq}} = \cos \epsilon \dot{I} - \sin \epsilon \dot{\Omega}, \quad (4)$$

$$\dot{\Omega}_{\text{eq}} = \sin \epsilon \dot{I} + \cos \epsilon \dot{\Omega}. \quad (5)$$

It is assumed that all the rates of changes appearing here and in the rest of the paper are averaged over the orbital period of the Earth's satellite and, when is the case, also over the period of an external third body; for the sake of simplicity, the angular brackets  $\langle \dots \rangle$  denoting the average are

---

<sup>5</sup>We assume  $\epsilon$  as constant.

omitted. By solving with respect to the ecliptical rates of change  $\dot{I}$ ,  $\dot{\Omega}$ , one finally gets

$$\dot{I} = \cos \epsilon \dot{I}_{\text{eq}} + \sin \epsilon \dot{\Omega}_{\text{eq}}, \quad (6)$$

$$\dot{\Omega} = -\sin \epsilon \dot{I}_{\text{eq}} + \cos \epsilon \dot{\Omega}_{\text{eq}}. \quad (7)$$

At this stage, there is nothing left to do but to express the known formulas for  $\dot{I}_{\text{eq}}$ ,  $\dot{\Omega}_{\text{eq}}$  in terms of the ecliptical elements  $I$ ,  $\Omega$ . To this aim, it is useful to calculate  $\cos I_{\text{eq}}$ ,  $\sin I_{\text{eq}}$ ,  $\cos \Omega_{\text{eq}}$ ,  $\sin \Omega_{\text{eq}}$  entering, e.g., the amplitudes of the tidal orbital perturbations. We have

$$\cos I_{\text{eq}} = \hat{\mathbf{S}}_{\text{eq}} \cdot \hat{\mathbf{n}}^{\text{eq}} = \cos I \cos \epsilon - \cos \Omega \sin I \sin \epsilon, \quad (8)$$

$$\sin^2 I_{\text{eq}} = |\hat{\mathbf{S}}_{\text{eq}} \times \hat{\mathbf{n}}^{\text{eq}}|^2 = (\cos \epsilon \cos \Omega \sin I + \cos I \sin \epsilon)^2 + \sin^2 I \sin^2 \Omega, \quad (9)$$

$$\cos \Omega_{\text{eq}} = \frac{\cos \epsilon \cos \Omega \sin I + \cos I \sin \epsilon}{\sin I_{\text{eq}}}, \quad (10)$$

$$\sin \Omega_{\text{eq}} = \frac{\sin I \sin \Omega}{\sin I_{\text{eq}}} \quad (11)$$

### 3. The Newtonian and post-Newtonian orbital rates of change

In the following, a circular orbit ( $e = 0$ ) will be considered.

#### 3.1. The post-Newtonian Lense-Thirring effect

The long-term Lense-Thirring rates of change of the inclination and the node valid in any coordinate system in which the  $\hat{k}_x$  component of the primary's symmetry axis vanishes are (Iorio 2011)

$$\dot{I}_{\text{LT}} = \frac{2GS \hat{k}_y \sin \Omega}{c^2 a^3}, \quad (12)$$

$$\dot{\Omega}_{\text{LT}} = \frac{2GS (\hat{k}_z + \hat{k}_y \cot I \cos \Omega)}{c^2 a^3}, \quad (13)$$

It should be noted that Equations (12) to (13) along with the following effects due to the geopotential (see Equations (14) to (20) below) are just a particular case of general expressions

valid in a completely arbitrary coordinate system in which  $\hat{\mathbf{k}}$  can assume any orientation in space (Iorio 2011; Renzetti 2013, 2014). If an ecliptical coordinate system is adopted, it can be demonstrated that the approach outlined in Section 2 yields the same results as those obtained by Iorio (2011); Renzetti (2013, 2014) for  $\hat{k}_x = 0$ ,  $\hat{k}_y = \sin \epsilon$ ,  $\hat{k}_z = \cos \epsilon$ .

Figures 1 to 2 depict the agreement between Equations (12) to (13) and the numerically integrated Lense-Thirring shifts which display just the expected linear temporal behaviour for the specific scenario  $I = \Omega = 90$  deg (see Section 3.2 for its relevance).

### 3.2. The Newtonian even and odd zonal harmonics of the geopotential

The classical long-term rates of change of the node due to the first even zonals are<sup>6</sup> (Iorio 2011; Renzetti 2013, 2014)

$$\dot{\Omega}_{J_2} = \frac{3}{2} n_b J_2 \left( \frac{R}{a} \right)^2 (\hat{k}_y \cos \Omega - \hat{k}_z \cot I) (\hat{k}_z + \hat{k}_y \cos \Omega \cot I) \sin I, \quad (14)$$

$$\dot{\Omega}_{J_3} = 0, \quad (15)$$

$$\begin{aligned} \dot{\Omega}_{J_4} = & -\frac{15}{64} n_b J_4 \left( \frac{R}{a} \right)^4 (\hat{k}_z + \hat{k}_y \cos \Omega \cot I) (\hat{k}_z \cos I - \hat{k}_y \cos \Omega \sin I) \times \\ & \times [5 - 7\hat{k}_z^2 + (7 - 21\hat{k}_z^2) \cos 2I + 14(-1 + \hat{k}_z^2) \cos 2\Omega \sin^2 I + 28\hat{k}_y \hat{k}_z \cos \Omega \sin 2I]. \end{aligned} \quad (16)$$

The classical long-term rates of change of the inclination due to the first even and odd zonals of low degree are (Iorio 2011; Renzetti 2013, 2014)

$$\dot{I}_{J_2} = \frac{3}{2} n_b J_2 \left( \frac{R}{a} \right)^2 \hat{k}_y (\hat{k}_y \sin I \cos \Omega - \hat{k}_z \cos I) \sin \Omega, \quad (17)$$

$$\dot{I}_{J_3} = 0, \quad (18)$$

$$\dot{I}_{J_4} = \frac{15}{128} n_b J_4 \left( \frac{R}{a} \right)^4 \hat{k}_y \{ -\hat{k}_y (-1 + 7\hat{k}_z^2) (5 + 7 \cos 2I) \sin I \sin 2\Omega +$$

---

<sup>6</sup>Eqs. (12)-(15) of Iorio (2011) yield Equation (17) and Equation (14) with the replacement  $Q_2 \rightarrow -GMR^2 J_2$ . It corrects a missing minus sign in Iorio (2011, p. 124001-4).

$$\begin{aligned}
 & + \hat{k}_z \cos I \left[ (-3 + 7\hat{k}_z^2) (1 + 7 \cos 2I) \sin \Omega - 42 (-1 + \hat{k}_z^2) \sin^2 I \sin 3\Omega \right] + \\
 & + 7\hat{k}_y (-1 + \hat{k}_z^2) \sin^3 I \sin 4\Omega \Big\}, \tag{19}
 \end{aligned}$$

$$\dot{I}_{J_5} = 0. \tag{20}$$

For a general value of the inclination, Equations (14) to (16) tells us that, if  $\Omega = 90$  deg, the node circulates with a secular precession given mainly by

$$\dot{\Omega} \simeq -\frac{3}{2} n_b J_2 \left( \frac{R}{a} \right)^2 \hat{k}_z^2 \cos I \left[ 1 - \frac{5}{8} \frac{J_4}{J_2} \left( \frac{R}{a} \right)^2 (-3 + 7\hat{k}_z^2 \cos^2 I) \right]. \tag{21}$$

This implies that the inclination undergoes both relativistic and classical long-periodic, harmonic variations whose frequencies are  $j\dot{\Omega}$ ,  $j = 1, 2, 3 \dots$ . In particular, there are some components of Equations (17) to (20), proportional to  $\hat{k}_y \hat{k}_z \cos I \sin \Omega$ , which have the same temporal pattern of Equation (12). Thus, they act as a potentially insidious systematic bias depending on the level of mismodeling in the zonal harmonics. The same holds also for Equation (13), impacted by the mismodelled part of Equation (21).

On the other hand, if the orbital plane is perpendicular to the ecliptic ( $I = 90$  deg), by choosing the initial value  $\Omega = 90$  deg allows to:

- (a) Keep the node essentially constant, as per

$$\dot{\Omega}_{J_2} = \frac{3}{2} n_b J_2 \left( \frac{R}{a} \right)^2 \hat{k}_z \hat{k}_y \cos \Omega, \tag{22}$$

$$\dot{\Omega}_{J_4} = \frac{15}{32} n_b J_4 \left( \frac{R}{a} \right)^4 \hat{k}_z \hat{k}_y \left[ -1 + 7\hat{k}_z^2 + 7(-1 + \hat{k}_z^2) \cos 2\Omega \right] \cos \Omega \tag{23}$$

which are obtained from Equations (14) to (16) for  $I = 90$  deg.

- (b) Maximize the Lense-Thirring rates of change which becomes secular trends, as per Equations (12) to (13)
- (c) Cancel all the classical rates of change on the inclination due to the static part of the



geopotential, as per

$$\dot{I}_{J_2} = \frac{3}{4}n_b \left(\frac{R}{a}\right)^2 \hat{k}_y^2 J_2 \sin 2\Omega, \quad (24)$$

$$\dot{I}_{J_3} = 0, \quad (25)$$

$$\dot{I}_{J_4} = \frac{15}{64}n_b \left(\frac{R}{a}\right)^4 J_4 (1 - \hat{k}_z^2) \left[-1 + 7\hat{k}_z^2 + 7(-1 + \hat{k}_z^2) \cos 2\Omega\right] \sin 2\Omega, \quad (26)$$

$$\dot{I}_{J_5} = 0, \quad (27)$$

which come from Equations (17) to (20) for  $I = 90$  deg.

Figure 3, obtained by numerically integrating the equations of motion with the accelerations due to the first five zonals of the geopotential, shows that, actually, the node and the inclination stay constant to their initial values if  $\Omega = I = 90$  deg are adopted for them.

In order to cope with the unavoidable orbital injection errors inducing departures from the chosen ideal orbital geometry, in Figures 4 to 5 we numerically investigate the impact of offsets of the order of  $\Delta\Omega = \Delta I = 0.1 - 0.01$  deg from the proposed scenario characterized by  $\Omega = I = 90$  deg for different altitudes of the satellite. Since the largest contribution to the classical inclination rate is due to  $J_2$ , the level of mismodeling in it plays a crucial role in determining the largest admissible deviations from the nominal orbital configuration. According to Iorio (2012a), who relies upon the method proposed by Wagner & McAdoo (2012) to realistically compare geopotential harmonics in recent and past gravitational fields, a conservative evaluation of the actual uncertainty in the first even zonal points toward  $\delta\bar{C}_{2,0} \simeq 3 \times 10^{-11} - 2 \times 10^{-10}$ . It should be remarked that the simple confrontation between the estimated values of  $J_2$  in some pairs of recent global gravity field solutions such as<sup>7</sup> IGGT\_R1, IfE\_GOCE05s, NULP-02S, GO\_CONS\_GCF\_2\_SPW\_R5 may yield figures as large as even  $\Delta\bar{C}_{2,0} \simeq 2 \times 10^{-9}$  (IGGT\_R1 vs. IfE\_GOCE05s). On the other hand, the formal, statistical errors  $\sigma_{\bar{C}_{2,0}}$  released in several global gravity models are as little as  $\simeq 10^{-12} - 10^{-13}$ . By assuming  $\delta\bar{C}_{2,0} = 2 \times 10^{-10}$ , Figures 1 to 2 and Figures 4 to 5 show that  $\Delta\Omega = \Delta I = 0.01$  deg allow to reach a  $\simeq 3 - 5 \times 10^{-3}$  level of systematic error in the Lense-Thirring effect for any altitude considered, while for  $\Delta\Omega, \Delta I = 0.1$  deg, the bias amounts to  $\simeq 3 - 5 \times 10^{-2}$ . It is interesting to remark that the deviations from the ideal polar orbit of the Gravity Probe B (GP-B) spacecraft were as little as  $5 \times 10^{-5}$  deg at its launch (Kahn 2007, p. 141); our constraints are much less demanding.

---

<sup>7</sup>They can be retrieved at the section Static Models of the WEB page of the International Center for Global Earth Models (ICGEM) at [http://icgem.gfz-potsdam.de/tom\\_longtime](http://icgem.gfz-potsdam.de/tom_longtime).

## 4. The tidal perturbations

### 4.1. the solid tides

The long-term perturbations due to the solid component of the  $\ell = 2$ ,  $m = 1$ ,  $p = 1$ ,  $q = 0$  constituent of the tesseral tide  $K_1$  on the satellite's inclination and node, referred to the equator, are

$$\dot{I}_{\text{eq}}^{K_1,s} = -\sqrt{\frac{5}{24\pi}} \frac{3g_{\oplus} R_{\oplus}^3 k_{2,1,K_1}^{(0)} H_2^1(K_1) \cos I_{\text{eq}}}{2n_b a^5} \sin(\Omega_{\text{eq}} - \delta_{2,1,K_1}), \quad (28)$$

$$\dot{\Omega}_{\text{eq}}^{K_1,s} = \sqrt{\frac{5}{24\pi}} \frac{3g_{\oplus} R_{\oplus}^3 k_{2,1,K_1}^{(0)} H_2^1(K_1) (1 - 2 \cos^2 I_{\text{eq}})}{2n_b a^5 \sin I_{\text{eq}}} \cos(\Omega_{\text{eq}} - \delta_{2,1,K_1}). \quad (29)$$

They can be calculated by applying the Lagrange planetary equations for the rates of change of the inclination and the node (Bertotti, Farinella & Vokrouhlický 2003) to Eq. (18) of Iorio (2001). According to Equations (6) to (7), the solid  $K_1$ -induced rate of changes of the inclination and node, referred to the ecliptic, are

$$\begin{aligned} \dot{I}^{K_1,s} = & \sqrt{\frac{5}{24\pi}} \frac{3g_{\oplus} R_{\oplus}^3 k_{2,1,K_1}^{(0)} H_2^1(K_1)}{2n_b a^5} \left[ -\cos \epsilon \cos I_{\text{eq}} (\sin \Omega_{\text{eq}} \cos \delta_{2,1,K_1} - \right. \\ & - \cos \Omega_{\text{eq}} \sin \delta_{2,1,K_1}) + \sin \epsilon \left( \frac{1 - 2 \cos^2 I_{\text{eq}}}{\sin I_{\text{eq}}} \right) (\cos \Omega_{\text{eq}} \cos \delta_{2,1,K_1} + \\ & \left. + \sin \Omega_{\text{eq}} \sin \delta_{2,1,K_1}) \right], \end{aligned} \quad (30)$$

$$\begin{aligned} \dot{\Omega}^{K_1,s} = & \sqrt{\frac{5}{24\pi}} \frac{3g_{\oplus} R_{\oplus}^3 k_{2,1,K_1}^{(0)} H_2^1(K_1)}{2n_b a^5} \left[ \sin \epsilon \cos I_{\text{eq}} (\sin \Omega_{\text{eq}} \cos \delta_{2,1,K_1} - \right. \\ & - \cos \Omega_{\text{eq}} \sin \delta_{2,1,K_1}) + \cos \epsilon \left( \frac{1 - 2 \cos^2 I_{\text{eq}}}{\sin I_{\text{eq}}} \right) (\cos \Omega_{\text{eq}} \cos \delta_{2,1,K_1} + \\ & \left. + \sin \Omega_{\text{eq}} \sin \delta_{2,1,K_1}) \right] \end{aligned} \quad (31)$$

in which Equations (8) to (11) are to be used to express Equations (30) to (31) in terms of the ecliptical orbital elements.

An alternative approach to straightforwardly obtain Equations (30) to (31) consists of expressing the perturbing tidal potential of Eq. (18) of Iorio (2001) for the solid component of  $K_1$

with  $\ell = 2$ ,  $m = 1$ ,  $p = 1$ ,  $q = 0$  in terms of the ecliptical orbital elements and, then, applying the Lagrange planetary equations, which are not restricted to any coordinate system, to them. In this way, it is also possible to straightforwardly infer that, in the case  $I = \Omega = 90$  deg, the long-term perturbations due to the zonal constituent 055.565 with  $\ell = 2$ ,  $m = 0$ ,  $p = 1$ ,  $q = 0$  vanish for both the inclination and the node.

In the ideal case  $e = 0$ ,  $I = \Omega = 90$  deg, Equations (30) to (31) become

$$i^{K_1,s} = \sqrt{\frac{5}{24\pi}} \frac{3g_{\oplus} R_{\oplus}^3 k_{2,1,K_1}^{(0)} H_2^1(K_1) \sin \delta_{2,1,K_1} \sin \epsilon}{2n_b a^5}, \quad (32)$$

$$\dot{\Omega}^{K_1,s} = \sqrt{\frac{5}{24\pi}} \frac{3g_{\oplus} R_{\oplus}^3 k_{2,1,K_1}^{(0)} H_2^1(K_1) \sin \delta_{2,1,K_1} \cos \epsilon}{2n_b a^5}, \quad (33)$$

## 4.2. The ocean tides

As far as the ocean component of the  $\ell = 2$ ,  $m = 1$ ,  $p = 1$ ,  $q = 0$   $K_1$  tidal line are concerned, we have

$$i_{\text{eq}}^{K_1,\text{oc}} = \frac{6G\rho_w R_{\oplus}^4 (1 + k_2') C_{2,1,K_1}^+ \cos I_{\text{eq}}}{5n_b a^5 (1 - e^2)^2} \cos(\Omega_{\text{eq}} - \varepsilon_{2,1,K_1}^+), \quad (34)$$

$$\dot{\Omega}_{\text{eq}}^{K_1,\text{oc}} = \frac{6G\rho_w R_{\oplus}^4 (1 + k_2') C_{2,1,K_1}^+ (1 - 2 \cos^2 I_{\text{eq}})}{5n_b a^5 (1 - e^2)^2 \sin I_{\text{eq}}} \sin(\Omega_{\text{eq}} - \varepsilon_{2,1,K_1}^+). \quad (35)$$

They can be obtained with the Lagrange planetary equations applied to Eq. (46) of Iorio (2001). From Equations (6) to (7), applied to Equations (34) to (35), one gets

$$\begin{aligned} i_{\text{eq}}^{K_1,\text{oc}} = & \frac{6G\rho_w R_{\oplus}^4 (1 + k_2') C_{2,1,K_1}^+}{5n_b a^5 (1 - e^2)^2} \left[ \cos \epsilon \cos I_{\text{eq}} \left( \cos \Omega_{\text{eq}} \cos \varepsilon_{2,1,K_1}^+ + \sin \Omega_{\text{eq}} \sin \varepsilon_{2,1,K_1}^+ \right) + \right. \\ & \left. + \sin \epsilon \left( \frac{1 - 2 \cos^2 I_{\text{eq}}}{\sin I_{\text{eq}}} \right) \left( \sin \Omega_{\text{eq}} \cos \varepsilon_{2,1,K_1}^+ - \cos \Omega_{\text{eq}} \sin \varepsilon_{2,1,K_1}^+ \right) \right], \quad (36) \end{aligned}$$

$$\dot{\Omega}_{\text{eq}}^{K_1,\text{oc}} = \frac{6G\rho_w R_{\oplus}^4 (1 + k_2') C_{2,1,K_1}^+}{5n_b a^5 (1 - e^2)^2} \left[ -\sin \epsilon \cos I_{\text{eq}} \left( \cos \Omega_{\text{eq}} \cos \varepsilon_{2,1,K_1}^+ + \sin \Omega_{\text{eq}} \sin \varepsilon_{2,1,K_1}^+ \right) + \right.$$

$$+ \cos \epsilon \left( \frac{1 - 2 \cos^2 I_{\text{eq}}}{\sin I_{\text{eq}}} \right) \left( \sin \Omega_{\text{eq}} \cos \varepsilon_{2,1,K_1}^+ - \cos \Omega_{\text{eq}} \sin \varepsilon_{2,1,K_1}^+ \right) \Big]. \quad (37)$$

Also Equations (36) to (37) can be alternatively obtained by expressing Eq. (46) of Iorio (2001) for the ocean component of  $K_1$  with  $\ell = 2$ ,  $m = 1$ ,  $p = 1$ ,  $q = 0$  in terms of the ecliptical orbital elements and, then, using the Lagrange planetary equations.

For  $I = \Omega = 90$  deg, Equations (36) to (37) reduce to

$$j^{K_1, \text{oc}} = \frac{6G\rho_w R_\oplus^4 (1 + k_2') C_{2,1,K_1}^+ \cos \varepsilon_{2,1,K_1}^+ \sin \epsilon}{5n_b a^5}, \quad (38)$$

$$\dot{\Omega}^{K_1, \text{oc}} = \frac{6G\rho_w R_\oplus^4 (1 + k_2') C_{2,1,K_1}^+ \cos \varepsilon_{2,1,K_1}^+ \cos \epsilon}{5n_b a^5}. \quad (39)$$

### 4.3. The impact of the mismodeling in the tidal parameters

Figures 6 to 7 show the sensibility of Equations (30) to (31) and Equations (36) to (37), plotted as functions of the satellite's semimajor axis  $a$ , to departures of  $I$ ,  $\Omega$  from the ideal configuration  $I = \Omega = 90$  deg. By noting that the Love number  $k_{2,1,K_1}$  seems currently known at an accuracy level not better than<sup>8</sup>  $\simeq 10^{-3}$ , it turns out that not too large offsets  $\Delta\Omega$ ,  $\Delta I \simeq 0.05$  deg would be adequate to cope with the solid tidal perturbation; suffice it to say that, for GP-B, it was  $\Delta I_{\text{eq}} = 5 \times 10^{-5}$  deg at its launch (Kahn 2007, p. 141). On the other hand, the nominal ocean tidal perturbations are larger than the solid ones; such a discrepancy is due to the different values of their lag angles  $\delta_{2,1,K_1}$ ,  $\varepsilon_{2,1,K_1}^+$  so that, while  $\sin \delta_{2,1,K_1} \simeq -0.005$ , on the other hand it is  $\cos \varepsilon_{2,1,K_1}^+ \simeq 0.77$ . Thus, the present-day level of uncertainty in the ocean tidal height coefficient of  $K_1$  is of crucial importance to assess the level of aliasing which could be induced on the relativistic signatures. If one had to rely upon the old EGM96 model along with its  $4 \times 10^{-2}$  relative uncertainty in  $C_{2,1,K_1}^+$  (Lemoine et al. 1998), the bias on the Lense-Thirring signature would be at a  $\simeq 40 - 50\%$  level. However, several other global ocean tide models have been produced since then: CSR4.0 (Eanes & Schuler 1999) TPXO.6.2 (Egbert & Erofeeva 2002) GOT99 (Ray 1999) FES2004 (Lyard et al. 2006), EOT11a (Savcenko & Bosch 2012), EOT11ag (Mayer-Gürr et al. 2012). By a comparison among them, it does not seem unrealistic to assume a present-day relative uncertainty of the order of  $\simeq 10^{-3}$  for  $C_{2,1,K_1}^+$ . Indeed, by calculating mean and standard deviation of the values computed at <https://bowie.gsfc.nasa.gov/ggfc/tides/harmonics.html> from the models

---

<sup>8</sup>L. Petrov and R. Ray, personal communications, August 2018. Nonetheless, in Jagoda et al. (2018) a relative uncertainty as little as  $3 \times 10^{-4}$  was reported on a generic  $k_2$  Love number determined with the LAGEOS and LAGEOS II satellites.

TPXO.6.2 (Egbert & Erofeeva 2002), GOT99 (Ray 1999) and FES2004 (Lyard et al. 2006), a relative uncertainty of  $1.8 \times 10^{-3}$  is inferred. It would yield an aliasing level of the Lense-Thirring signatures of a few percent.

#### 4.4. The linear combination approach

At first sight, a possible way to overcome such an issue would consist of suitably designing a linear combination of the satellite's inclination and node which, by construction, cancels out both the ocean and solid tidal perturbations due to the  $K_1$  line. By means of Equations (38) to (39) it is possible to obtain

$$f \doteq \dot{I} + c_1 \dot{\Omega}, \quad (40)$$

with

$$c_1 = -\tan \epsilon = -0.433547. \quad (41)$$

Unfortunately, the linear combination of Equation (40) cancels out also the Lense-Thirring precessions; indeed, Equations (12) to (13) reduce just to

$$\dot{I}_{\text{LT}} = \frac{2GS \sin \epsilon}{c^2 a^3}, \quad (42)$$

$$\dot{\Omega}_{\text{LT}} = \frac{2GS \cos \epsilon}{c^2 a^3} \quad (43)$$

for  $e = 0$ ,  $I = \Omega = 90$  deg. It is a consequence of a general result about  $f$  which can be drawn for  $I = \Omega = 90$  deg for the perturbations induced by any disturbing acceleration. Indeed, from Equations (6) to (7) and Equations (40) to (41), it turns out that the combined signature for the inclination and node rates of change due to a generic perturbing acceleration  $A_{\text{pert}}$  of whatsoever physical origin, is

$$f^{\text{pert}} = \frac{\dot{I}_{\text{eq}}^{\text{pert}}}{\cos \epsilon}, \quad (44)$$

where the analytical expression for  $\dot{I}_{\text{eq}}^{\text{pert}}$  has to be evaluated for  $I = \Omega = 90$  deg. In the case of the Lense-Thirring effect, Equation (44) tells us immediately that  $f^{\text{LT}}$  vanishes since there is no gravitomagnetic precession for  $I$  in the equatorial coordinate system.

#### 5. The De Sitter precessions

On the other hand, Equations (40) to (41) has the advantage of returning a non-vanishing effect due to the post-Newtonian gravitoelectric De Sitter precessions of the satellite's inclination and node.

Indeed, by using Eq. (4) and Eq. (8) of Iorio (2018), which describe the geodetic rates of change of the satellite’s inclination and node with respect to any<sup>9</sup> coordinate system, in the scenario  $I = \Omega = 90$  deg, Equations (40) to (41) return

$$f^{\text{DS}} = -\frac{3\mu_{\odot}n_{\text{b}}^{\oplus}(\cos \Omega_{\oplus} \sin I_{\oplus} + \cos I_{\oplus} \tan \epsilon)}{2c^2a_{\oplus}(1 - e_{\oplus}^2)} = -8.31986 \text{ mas yr}^{-1}. \quad (45)$$

The signature of Equation (45) is essentially a secular trend since the inclination and the node of the heliocentric Earth’s orbit change over timescales of the order of  $\simeq 0.1 - 1$  Myr, as can be inferred by their extremely slow rates of change (Murray & Dermott 2000). It is important to remark that Equation (45) would not be affected, by construction, by the largest and most insidious among the tidal perturbations, i.e. the  $K_1$  tide; the zonal tide 055.565 is of no concern since in Section 4 it was shown that its long-term perturbations vanish for both the inclination and the node. Furthermore, also the static part of the geopotential would be of no concern, as previously shown in Section 3 for the inclination and the nodes taken separately. Figure 8 shows the impact of departures  $\Delta I = \Delta \Omega = 0.1$  deg from the condition  $I = \Omega = 90$  deg on the nominal zonals perturbations combined according to Equations (40) to (41). The corresponding mismodeled signatures would be completely negligible even by assuming very conservative levels of uncertainty in  $J_{\ell}$ ,  $\ell \geq 2$ .

## 6. The 3rd-body perturbations: the Sun and the Moon

The results of Iorio (2012b) concerning the rates of change of the satellite’s orbital elements, averaged over its orbital period  $P_{\text{b}}$ , induced by a distant perturber X can be straightforwardly used in the present context since they are valid in any coordinate system. The doubly averaged rate of change of the node can be obtained by averaging Eq. (9) of Iorio (2012b) over the orbital period  $P_{\text{X}}$  of the 3rd-body. The general result is

$$\begin{aligned} \dot{\Omega}^{\text{3rd body}} = & -\frac{3\mu_{\text{X}}}{8a_{\text{X}}^3 \sqrt{1 - e^2}(1 - e_{\text{X}}^2)^{3/2}n_{\text{b}}} [\cos I_{\text{X}} \cot I + \cos(\Omega - \Omega_{\text{X}}) \sin I_{\text{X}}] \times \\ & \times \left\{ -(-2 - 3e^2 + 5e^2 \cos 2\omega) [\cos I_{\text{X}} \sin I - \cos I \cos(\Omega - \Omega_{\text{X}}) \sin I_{\text{X}}] - \right. \\ & \left. - 5e^2 \sin I_{\text{X}} \sin 2\omega \sin(\Omega - \Omega_{\text{X}}) \right\}. \end{aligned} \quad (46)$$

---

<sup>9</sup>It is understood that it has to be intended as kinematically rotating (Brumberg & Kopeikin 1989).

Eq. (20) of Iorio (2018) and Equation (46), for  $e = 0$ ,  $I = \Omega = 90$  deg, reduce to

$$\dot{J}^{\text{3rd body}} = \frac{3\mu_X \sin^2 I_X \sin 2\Omega_X}{8a_X^3 (1 - e_X^2)^{3/2} n_b}, \quad (47)$$

$$\dot{\Omega}^{\text{3rd body}} = -\frac{3\mu_X \sin 2I_X \sin \Omega_X}{8a_X^3 (1 - e_X^2)^{3/2} n_b}, \quad (48)$$

which can be linearly combined according to Equations (40) to (41) giving

$$f^{\text{3rd body}} = \frac{3\mu_X \sin I_X \sin \Omega_X (\sin I_X \cos \Omega_X + \tan \epsilon \cos I_X)}{4a_X^3 (1 - e_X^2)^{3/2} n_b}. \quad (49)$$

As far as the Moon is concerned, its node, referred to the ecliptic, undergoes a secular precession with a period of  $T_{\Omega_{\mathcal{C}}} = 18.6$  yr; its current value is  $\Omega_{\mathcal{C}} = 125.1$  deg. Thus, although at the price of a long wait, Equations (47) to (49) will finally average out in view of their frequencies  $\dot{\Omega}_{\mathcal{C}}$ ,  $2\dot{\Omega}_{\mathcal{C}}$ , and it can be stated that they would be of no concern for either the individual Lense-Thirring precessions of Equations (12) to (13) and the combined De Sitter effect of Equation (45). Such a conclusion is true for each of the gravitomagnetic signatures also without waiting for the completion of a full cycle of the lunar node, as it can be easily checked by inspecting the maximum values of the mismodeled parts of Equations (47) to (48) for any value of  $a$  and comparing them to Figures 1 to 2. To this aim, we assumed a relative uncertainty in the selenocentric gravitational parameter of  $2 \times 10^{-8}$ , as per the Object Data Page of the Moon provided by the JPL HORIZONS Web interface, revised on 2013. The situation is subtler for the combined De Sitter trend in view of the higher level of accuracy pursued. The maximum impact on Equation (49) occurs when  $\Omega_{\mathcal{C}} = 90$  deg, so that

$$f_{\text{max}}^{\mathcal{C}} = \frac{3GM_{\mathcal{C}} \tan \epsilon \sin 2I_{\mathcal{C}}}{8a_{\mathcal{C}}^3 (1 - e_{\mathcal{C}}^2)^{3/2} n_b}. \quad (50)$$

In Figure 9 we plot the mismodeled part of Equation (50) as a function of  $a$ . It can be noted that it stays in the range  $\approx 3 - 10 \times 10^{-5}$  of Equation (45).

About the 3-body effect of the Sun, it is completely negligible. Indeed, it is

$$f_{\text{max}}^{\odot} \simeq \frac{M_{\odot}}{M_{\mathcal{C}}} \left( \frac{a_{\mathcal{C}}}{a_{\oplus}} \right)^3 \frac{\sin 2I_{\oplus}}{\sin 2I_{\mathcal{C}}} f_{\text{max}}^{\mathcal{C}} = 3 \times 10^{-4} f_{\text{max}}^{\mathcal{C}}. \quad (51)$$

Furthermore, the heliocentric gravitational parameter is currently known with a relative accuracy of  $7 \times 10^{-11}$  (Pitjeva 2015).

## 7. The non-gravitational perturbations

The long-term rates of change induced by the non-gravitational accelerations on the inclination and node, referred to the equator, of the LAGEOS-type satellites have been extensively investigated in the literature in the context of their bias on the equator-referred Lense-Thirring node precession by finding them at the percent level or less for LAGEOS. Thus, it is arguable that the same holds also when they are combined according to Equations (6) to (7) in order to yield their ecliptical counterparts. Indeed, the averaged node perturbations which vanish for  $e = 0$ ,  $I = \Omega = 90$  deg are those due to the Poynting-Robertson effect (Lhotka, Celletti & Gales 2016, p. 608), the infrared radiation pressure of the Earth (Sehna 1981, p. 176), the atmospheric drag (Milani, Nobili & Farinella 1987, p. 103), the hypothetical asymmetric reflectivity (Lucchesi 2002, Eq. (44), p. 1083), the geomagnetic field, as can be inferred by integrating the Gauss equation for the rate of change of the node by means of Abdel-Aziz & Khalil (2014, Eq. (24), p. 592), with  $1/\sin f$  in its first term corrected to  $\sin f$ , to zero order in  $e$  for  $I = 90$  deg, the secular trend due to the Yarkovsky-Rubincam effect (Lucchesi 2002, Eq. (19), p. 1075), the Earth albedo (Lucchesi 2001, Eq. (35), p. 456) and the solar radiation pressure (Lucchesi 2001, Eq. (18), p. 451) in absence of eclipses. In the case of eclipses, by using the first term in the series of Eq. (2) and Eq. (4) in Ferraz Mello (1972) for the shadow function it can be shown that, to zero order in  $e$ , the node rates due to the albedo and the solar radiation pressure do not vanish; nonetheless, they turn out to be proportional to  $\sin 2\lambda_{\odot}$ , which averages out after 1/2 yr. About the long-term signatures due to the Yarkovsky-Rubincam effect having the frequencies  $\dot{\Omega}$  (Lucchesi 2002, Eq. (18), p. 1075) and  $2\dot{\Omega}$  (Lucchesi 2002, Eq. (17), p. 1075), they vanish if the satellite's spin axis is perpendicular to the Earth's equator. The same holds for the secular rate due to the Yarkovsky-Schach effect (Lucchesi 2002, Eq. (34), p. 1079). A similar situation occurs for the inclination, as shown in Sec. (6) of Iorio (2018).

As far as the De Sitter effect is concerned, by recalling the general result of Equation (44), all the findings of Sec. (6) of Iorio (2018) retain their validity, pointing towards an impact of the non-gravitational perturbations on the combined De Sitter trend of Equation (45) globally meeting our requirement.

## 8. A comparison with the counter-orbiting scenario by van Patten and Everitt

Some decades ago, it was proposed by van Patten and Everitt (vPE) to launch a pair of counter-orbiting drag-free spacecraft in nearly identical circular and polar orbits at an altitude of about 800 km to perform a  $\simeq 1\%$  measurement of both the Lense-Thirring and De Sitter node precessions by monitoring the sum of their nodes (van Patten & Everitt 1976b,a; Schaechter et al. 1977; van Patten et al. 1978). In addition to the drag-free apparatus to counteract the non-gravitational perturbations, the vPE's satellites should have been endowed also with the capability of reciprocal Doppler tracking at mutual encounters when passing over the poles. Careful arrangements to avoid in-orbit collisions would have been required as well (Schaechter et al.



1976). The main, striking differences between ELXIS and the vPE’s proposal are as follows

- a) The ELXIS concept is based on just a single satellite instead of two spacecraft, as in the vPE’s proposal.
  - $a^I$ ) ELXIS should not be necessarily too complex and/or expensive since a comparatively simpler, well manufactured cannonball geodetic satellite of LAGEOS-type would likely fit our accuracy requirements since, as we have demonstrated, most of the non-gravitational perturbations vanish or average out after more or less long temporal intervals. Moreover, once in orbit, ELXIS could well wait for forthcoming improvements in both the tracking accuracy and in dynamical modeling of, e.g., the ocean tides, thus by allowing for repeated tests with likely continuously improved accuracy over the subsequent years.
  - $a^{II}$ ) There are no particular limitations on the orbital height, which can be conveniently set according to the unavoidable engineering/budgetary trade-off.
  - $a^{III}$ ) There are no collision-related issues.
  - $a^{IV}$ ) No careful satellite-to-satellite measurements of the angle between the two orbital planes at the poles are present.
- b) While van Patten & Everitt (1976b) proposed to make a combined Lense-Thirring + De Sitter test, ELXIS would allow to perform separate-and even redundant-measurements of such two general relativistic effects. The De Sitter effect can be disentangled from the Lense-Thirring one both in the equatorial and in the ecliptical coordinate systems. Indeed, in the first case (Iorio 2018), based on the analysis of the satellite’s inclination only, the Lense-Thirring rate of change of it vanishes for  $\hat{k}_x = \hat{k}_y = 0$ , while in the second case, the linear combination of Equations (40) to (41) cancels out just the gravitomagnetic precessions and enforces the geodetic ones yielding Equation (45). Conversely, the Lense-Thirring measurements could be easily made independently of the geodetic effect itself simply by using an ecliptical version of the standard kinematically non-rotating and dynamically rotating geocentric coordinate system in which the De Sitter precession is automatically accounted for, not showing up in spacecraft motions. Basically, it would be just a geometrically rotated version of the usual ICRS adopted for routinely analyzing Earth’s satellites data.
- c) With ELXIS, the accuracy in measuring the De Sitter combined precessions, independently of the Lense-Thirring effect, would be of the order of  $\simeq 10^{-5}$ , while (van Patten & Everitt 1976b) claimed a  $\simeq 1\%$  accuracy in a mixed measurement of both the Lense-Thirring and the geodetic precessions. On the other hand, van Patten & Everitt (1976a) wrote that they could have obtained an independent test of the De Sitter effect at 10%, i.e. about 4 orders of magnitude worse than what could be obtained with ELXIS.
- d) The orbit injection errors on the nodes  $\Omega$  of the vPE’s satellites should have been of the order of 0.03 deg (van Patten & Everitt 1976a), which is a figure comparable with the ELXIS

case, although offsets up to 0.1 deg would not compromise our accuracy goals. On the other hand, the requirements by van Patten & Everitt (1976a) on the inclinations of the orbital planes would have been of the order of  $\approx 0.0008$  deg, while for ELXIS they are at the  $\approx 0.01 - 0.1$  deg level.

- e) A major drawback of the error budget of van Patten & Everitt (1976b,a) is that they seemingly did not take into account the perturbations due to the ocean tides induced on the satellites' motions by the free space tidally distorted Earth's potential. It is difficult to think that, say, the  $K_1$  tide may have had no substantial effects on the vPE's spacecraft in view of the results obtained in the present study and of the fact that, at the time of van Patten & Everitt (1976b,a), the first, relatively rudimentary satellite-based global ocean tide models, if any, were much less accurate than now. Suffice it to say that Felsentreger, Marsh & Agreen (1976) released errors in ocean tidal height  $C_{2,1,K_1}^+$  as large as  $\approx 8 - 28\%$ . Moreover, the uncertainty in it from the global Earth's gravity field model GEM-T3S (Lerch et al. 1992), published about 15 yr after the vPE's proposal, was still 6%.

Thus, it is clear that, even by limiting ourselves to the point *a*) and assuming hypothetically the same accuracy goals, ELXIS should be deemed as better than the vPE's proposal. Moreover, even by pessimistically surmising that our evaluation of the actually obtainable accuracy on the De Sitter measurement should be moved to, say, the  $\approx 10^{-4}$  level, it would still be 3 orders of magnitude better than 10% (van Patten & Everitt 1976a).

## 9. Summary and conclusions

Using a geocentric kinematically rotating ecliptical coordinate system to analyze the data of a single Earth's satellite, provisionally named ELXIS, placed in a circular orbit perpendicular to the equator and to the reference direction of the Vernal Equinox has the advantage of allowing to use both its inclination and node to measure the general relativistic Lense-Thirring and De Sitter effects without being impacted by the competing classical long-term precessions due to the even and odd zonals of the geopotential, which ideally vanish. On the other hand, the ocean component of the  $K_1$  tide induces aliasing perturbations which may degrade the accuracy of the proposed recovery of the individual gravitomagnetic and geodetic signatures. Depending on the actual mismodeling in the global ocean tide models, their impact on each of the Lense-Thirring rates may be at the percent level, representing the most limiting factor in measuring them. It is not unrealistic to expect further improvements in the forthcoming global tide solutions; in any case, once the satellite is in orbit, it would always be possible to wait just enough for the tidal models to reach the required accuracy. Moreover, it should be recalled that, after all, the accuracy of GP-B, which is the only uncontroversial test of the Earth's gravitomagnetic field published so far, is 19%. As far as the De Sitter effect is concerned, the goal of a  $\approx 10^{-5}$  accuracy of its measurement can be enforced with respect to an equatorial frame by linearly combining its geodetic precessions on the satellite's inclination and node in such a way to cancel out, by construction, the solid

and tidal perturbations due to the  $K_1$  and other tides. The impact of the combined 3rd-body perturbations due to the Moon, which are relevant only for the De Sitter test at the considered level of accuracy, averages out after 18.6 yr since the smallest characteristic frequency of their combined signatures is just that of the lunar node. However, given the current level of uncertainty in the selenocentric gravitational parameter, the largest bias during a full cycle of it would be no larger than  $\simeq 3 \times 10^{-5} - 1 \times 10^{-4}$ . The non-gravitational perturbations, preliminarily examined by assuming a cannonball geodetic satellite of LAGEOS-type, should not be a concern. Such conclusions hold substantially for any value of the satellite’s semimajor axis and for departures as large as  $\simeq 0.01 - 0.1$  deg from the ideal orbital geometry proposed.

### Acknowledgements

I am grateful to S. Kopeikin for some important clarifications and to an anonymous referee for the idea of comparing the present proposal with a past one.

### Appendix A Notations and definitions

Here, some basic notations and definitions used in the text are presented. For the numerical values of some of them, see Table 1. The orbital elements referred to the mean Earth’s equator at the reference epoch J2000.0 are denoted with the subscript “eq” in the main text.

$G$  : Newtonian constant of gravitation

$c$  : speed of light in vacuum

$\epsilon$  : mean obliquity

$M_{\oplus}$  : mass of the Earth

$\mu_{\oplus} \doteq GM_{\oplus}$  : gravitational parameter of the Earth

$S_{\oplus}$  : magnitude of the angular momentum of Earth

$\hat{\mathbf{S}}_{\oplus} = \{0, \sin \epsilon, \cos \epsilon\}$  : spin axis of the Earth in an ecliptic coordinate system

$R_{\oplus}$  : equatorial radius of the Earth

$\overline{C}_{\ell,m}$  : fully normalized Stokes coefficient of degree  $\ell$  and order  $m$  of the multipolar expansion of the Earth’s gravitational potential

$J_{\ell} = -\sqrt{2\ell+1} \overline{C}_{\ell,0}$  : zonal harmonic coefficient of degree  $\ell$  of the multipolar expansion of the Earth’s gravitational potential

$g_{\oplus}$  : Earth's acceleration of gravity at the equator

$k_{2,1,K_1}^{(0)}$  : dimensionless frequency-dependent Love number for the  $K_1$  tidal constituent of degree  $\ell = 2$  and order  $m = 1$

$H_2^1(K_1)$  : frequency-dependent solid tidal height for the  $K_1$  constituent of degree  $\ell = 2$  and order  $m = 1$

$\delta_{2,1,K_1}$  : phase lag of the response of the solid Earth with respect to the constituent  $K_1$  of degree  $\ell = 2$  and order  $m = 1$ .

$\rho_w$  : volumetric ocean water density

$k_2'$  : dimensionless load Love number

$C_{2,1,K_1}^+$  : ocean tidal height for the constituent  $K_1$  of degree  $\ell = 2$  and order  $m = 1$ .

$\varepsilon_{2,1,K_1}^+$  : phase shift due to hydrodynamics of the oceans for the tidal constituent  $K_1$  of degree  $\ell = 2$  and order  $m = 1$ .

$\mathbf{r}$  : satellite's position vector with respect to the Earth

$r$  : magnitude of the satellite's position vector with respect to the Earth

$a$  : semimajor axis of the geocentric satellite's orbit

$n_b \doteq \sqrt{\mu_{\oplus} a^{-3}}$  : Keplerian mean motion of the geocentric satellite's orbit

$P_b \doteq 2\pi n_b^{-1}$  : orbital period of the geocentric satellite's orbit

$e$  : eccentricity of the geocentric satellite's orbit

$I$  : inclination of the orbital plane of the geocentric satellite's orbit to the mean ecliptic at the reference epoch J2000.0

$\Omega$  : longitude of the ascending node of the geocentric satellite's orbit referred to the mean ecliptic at the reference epoch J2000.0

$\hat{\mathbf{n}} = \{\sin I \sin \Omega, -\sin I \cos \Omega, \cos I\}$  : normal unit vector in an ecliptic coordinate system. It is perpendicular to the satellite's orbital plane

$M_{\odot}$  : mass of the Sun

$\mu_{\odot} \doteq GM_{\odot}$  : gravitational parameter of the Sun

$a_{\oplus}$  : semimajor axis of the heliocentric Earth's orbit

$n_b^{\oplus} \doteq \sqrt{\mu_{\odot} a_{\oplus}^{-3}}$  : Keplerian mean motion of the heliocentric Earth's orbit

$P_{\oplus} \doteq 2\pi n_{\oplus}^{-1}$  : orbital period of the heliocentric Earth's orbit

$e_{\oplus}$  : eccentricity of the heliocentric Earth's orbit

$I_{\oplus}$  : inclination of the orbital plane of the heliocentric Earth's orbit to the mean ecliptic at the reference epoch J2000.0

$\dot{I}_{\oplus}$  : frequency of the inclination of the heliocentric Earth's orbit referred to the mean ecliptic at the reference epoch J2000.0

$\Omega_{\oplus}$  : longitude of the ascending node of the heliocentric Earth's orbit referred to the mean ecliptic at the reference epoch J2000.0

$\dot{\Omega}_{\oplus}$  : frequency of the node of the heliocentric Earth's orbit referred to the mean ecliptic at the reference epoch J2000.0

$M_X$  : mass of the 3rd body X (Sun  $\odot$  or Moon  $\lrcorner$  )

$\mu_X \doteq GM_X$  : gravitational parameter of the 3rd body X (Sun  $\odot$  or Moon  $\lrcorner$  )

$a_X$  : semimajor axis of the geocentric orbit of the 3rd body X

$P_X$  : orbital period of the geocentric orbit of the 3rd body X

$e_X$  : eccentricity of the geocentric orbit of the 3rd body X

$I_X$  : inclination of the orbital plane of the geocentric orbit of the 3rd body X to the mean ecliptic at the reference epoch J2000.0

$\Omega_X$  : longitude of the ascending node of the geocentric orbit of the 3rd body X referred to the mean ecliptic at the reference epoch J2000.0

$T_{\Omega_{\lrcorner}}$  : period of the node of the geocentric Moon's orbit referred to the mean ecliptic at the reference epoch J2000.0

## Appendix B Tables and Figures

Table 1: Relevant physical and orbital parameters used in the text. Most of the reported values come from Iorio (2001); Petit, Luzum & et al. (2010) and references therein. The source for the orbital elements characterizing the heliocentric orbit of the Earth, referred to the mean ecliptic at the reference epoch J2000.0, is the freely consultable database JPL HORIZONS on the Internet at <https://ssd.jpl.nasa.gov/?horizons> from which they were retrieved by choosing the time of writing this paper as input epoch. For the level of accuracy with which some of the parameters listed here are currently known, see the main text.

Parameter	Units	Numerical value
$G$	$\text{kg m}^3 \text{s}^{-2}$	$6.67259 \times 10^{-11}$
$c$	$\text{m s}^{-1}$	$2.99792458 \times 10^8$
$\epsilon$	deg	23.4393
$\mu_{\oplus}$	$\text{m}^3 \text{s}^{-2}$	$3.986004418 \times 10^{14}$
$S_{\oplus}$	$\text{kg m}^2 \text{s}^{-1}$	$5.86 \times 10^{33}$
$R_{\oplus}$	m	$6.3781366 \times 10^6$
$\overline{C}_{2,0}$	–	$-4.84165299806 \times 10^{-4}$
$g_{\oplus}$	$\text{m s}^{-2}$	9.7803278
$k_{2,1,K_1}^{(0)}$	–	0.257
$H_2^1(K_1)$	m	0.3687012
$\delta_{2,1,K_1}$	deg	–0.3
$\rho_w$	$\text{kg m}^{-3}$	$1.025 \times 10^3$
$k_2'$	–	–0.3075
$C_{2,1,K_1}^+$	m	$2.23659 \times 10^{-2}$
$\varepsilon_{2,1,K_1}^+$	deg	315.958
$\mu_{\odot}$	$\text{m}^3 \text{s}^{-2}$	$1.32712440018 \times 10^{20}$
$a_{\oplus}$	au	1.000003360971446
$e_{\oplus}$	–	0.01636541170625853
$I_{\oplus}$	deg	0.003786566401597615
$\dot{I}_{\oplus}$	deg cty $^{-1}$	–0.01337178
$\Omega_{\oplus}$	deg	171.6446280787646
$\dot{\Omega}_{\oplus}$	deg cty $^{-1}$	–0.24123856
$\mu_{\zeta}$	$\mu_{\oplus}$	$1.23000371 \times 10^{-2}$
$a_{\zeta}$	km	385,734
$e_{\zeta}$	–	0.05183692147447081
$I_{\zeta}$	deg	5.208682439763778
$\Omega_{\zeta}$	deg	125.1041727302047
$T_{\Omega_{\zeta}}$	yr	18.6

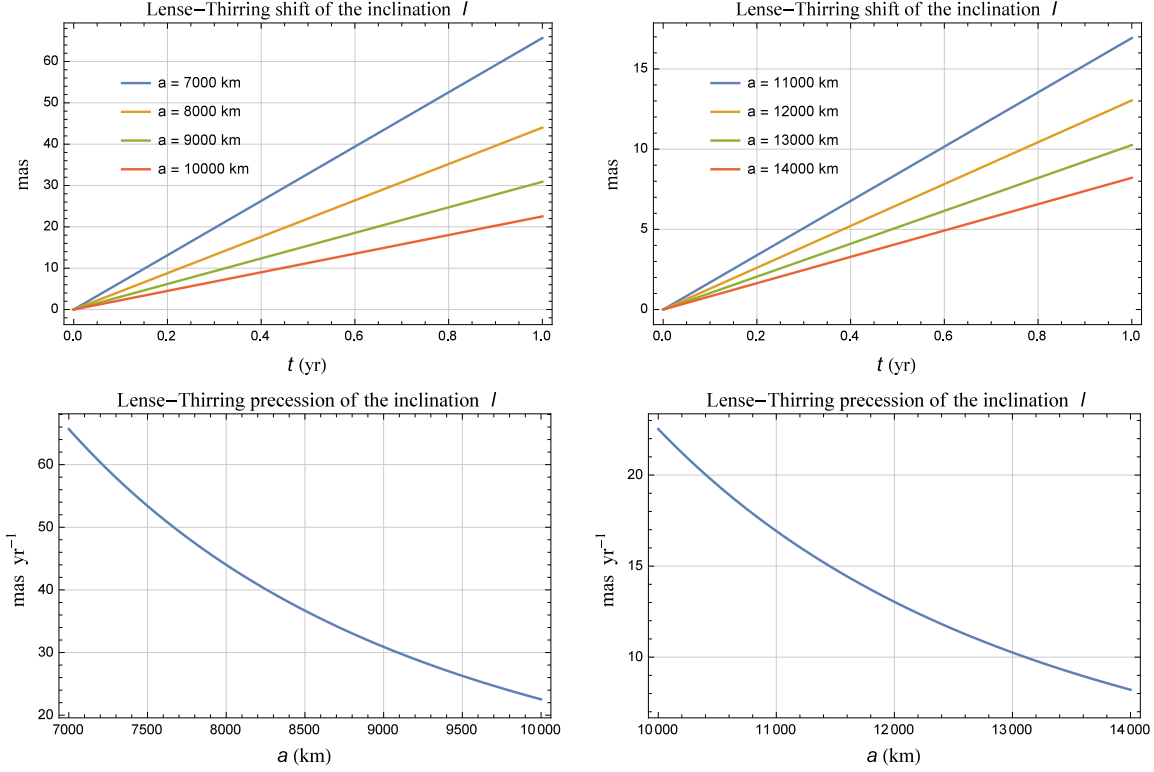


Fig. 1.— Upper row: annual Lense-Thirring shifts of the satellite’s inclination  $I$  obtained for different values of  $a$  by subtracting two time series produced by numerically integrating the equations of motion in rectangular Cartesian coordinates with and without the gravitomagnetic acceleration. Both the runs shared the same initial conditions characterized, among other things, by  $e = 0, \Omega = I = 90$  deg. Lower row: Plot of the Lense-Thirring rate of change of the satellite’s inclination  $I$  as a function of the semimajor axis  $a$  calculated analytically from Equation (12) for  $e = 0, \Omega = I = 90$  deg. In both cases, a reference frame with the mean ecliptic at the epoch J2000.0 was used as reference  $\{x, y\}$  plane so that  $\hat{k}_x = 0$ ,  $\hat{k}_y = \sin \epsilon = 0.3978$ ,  $\hat{k}_z = \cos \epsilon = 0.9175$ .

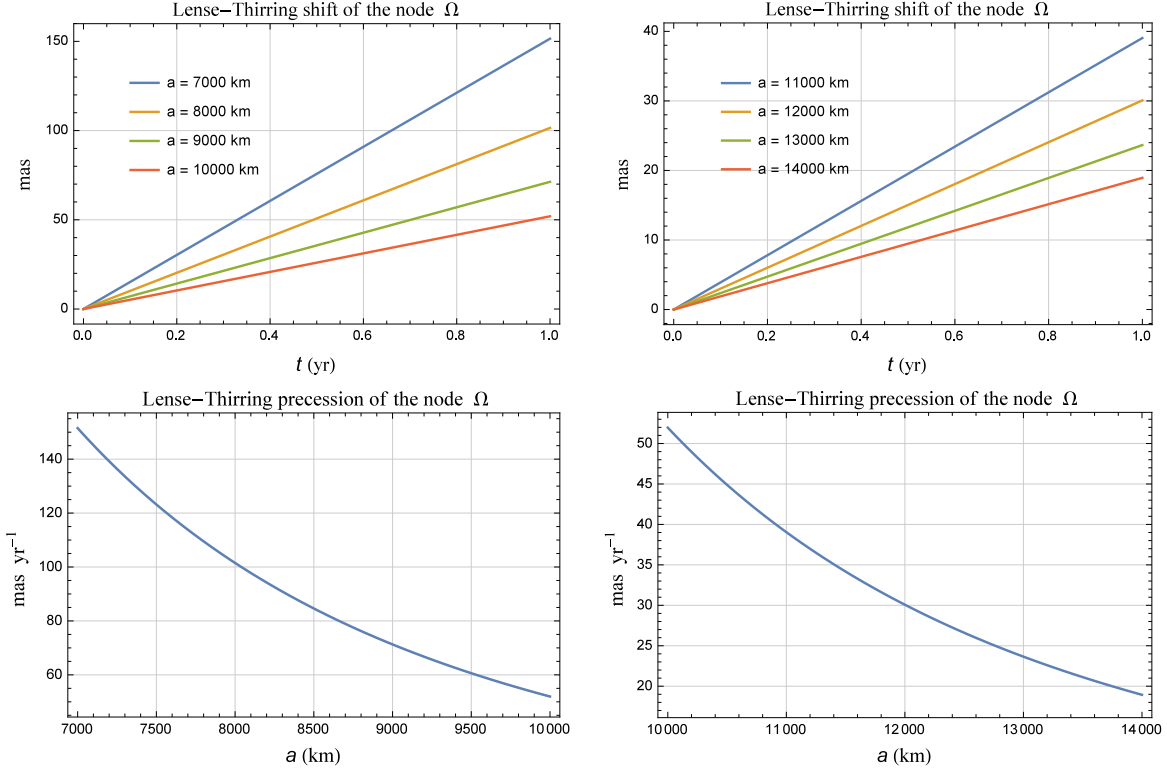


Fig. 2.— Upper row: annual Lense-Thirring shifts of the satellite’s node  $\Omega$  obtained for different values of  $a$  by subtracting two time series produced by numerically integrating the equations of motion in rectangular Cartesian coordinates with and without the gravitomagnetic acceleration. Both the runs shared the same initial conditions characterized, among other things, by  $e = 0, \Omega = I = 90$  deg. Lower row: Plot of the Lense-Thirring rate of change of the satellite’s node  $\Omega$  as a function of the semimajor axis  $a$  calculated analytically from Equation (13) for  $e = 0, \Omega = I = 90$  deg. In both cases, a reference frame with the mean ecliptic at the epoch J2000.0 was used as reference  $\{x, y\}$  plane so that  $\hat{k}_x = 0$ ,  $\hat{k}_y = \sin \epsilon = 0.3978$ ,  $\hat{k}_z = \cos \epsilon = 0.9175$ .



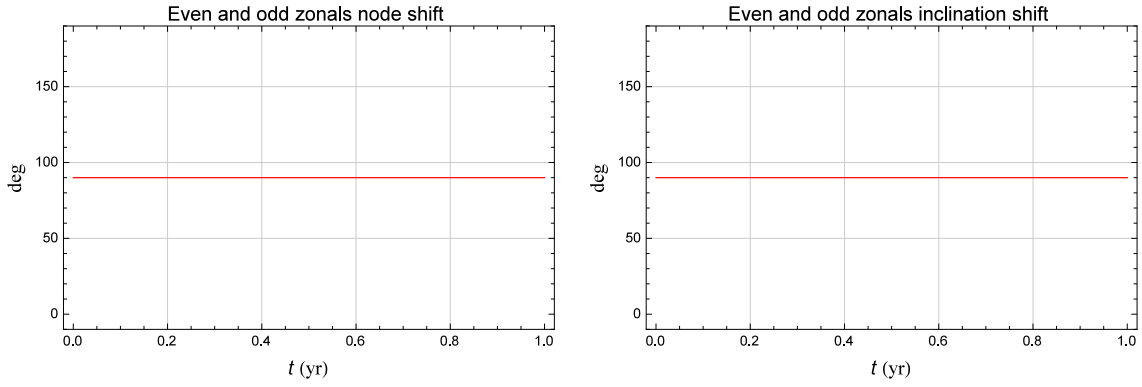


Fig. 3.— Annual shifts of the satellite’s node  $\Omega$  (left panel) and inclination  $I$  (right panel) obtained, for each orbital element, by subtracting two time series produced by numerically integrating the equations of motion in rectangular Cartesian coordinates with and without the classical accelerations due to the first five even zonal harmonics  $J_2$ ,  $J_3$ ,  $J_4$ ,  $J_5$ ,  $J_6$  of the geopotential. For each orbital element, both the runs shared the same initial conditions characterized, among other things, by  $e = 0$ ,  $\Omega = I = 90$  deg. The meaning of the plots displayed is that if the satellite’s node and inclination are set to such initial values, they stay constant to them throughout the orbital evolution. The result turns out to be independent of the semimajor axis  $a$ . A reference frame with the mean ecliptic at the epoch J2000.0 was used as reference  $\{x, y\}$  plane so that  $\hat{k}_x = 0$ ,  $\hat{k}_y = \sin \epsilon = 0.3978$ ,  $\hat{k}_z = \cos \epsilon = 0.9175$ .

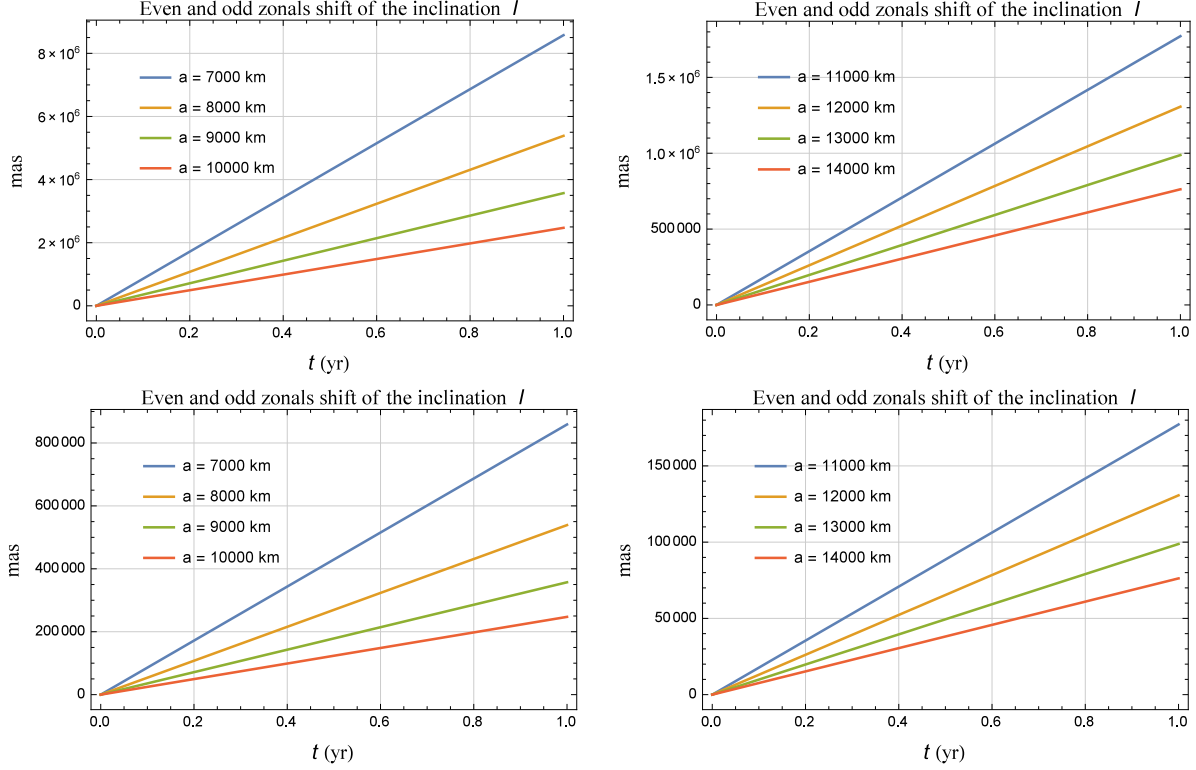


Fig. 4.— Upper row: nominal annual shifts of the satellite’s inclination  $I$  obtained for different values of  $a$  by subtracting two time series produced by numerically integrating the equations of motion in rectangular Cartesian coordinates with and without the classical accelerations due to the first five even zonal harmonics  $J_2, J_3, J_4, J_5, J_6$  of the geopotential. Both the runs shared the same initial conditions characterized, among other things, by  $e = 0, \Omega = I = 90 \pm 0.1$  deg. Lower row: same as in the upper row, apart from an offset of 0.01 deg from the ideal condition  $I = \Omega = 90$  deg. The largest contribution is due to  $J_2$ , whose present-day uncertainty may be as large as  $\lesssim 2 \times 10^{-10}$  if evaluated conservatively; the statistical, formal errors  $\sigma_{\bar{C}_{2,0}}$  released in the global gravity field models produced from the GRACE/GOCE data by several institutions around the world are even  $\simeq 1 - 3$  orders of magnitude smaller. In both cases, a reference frame with the mean ecliptic at the epoch J2000.0 was used as reference  $\{x, y\}$  plane so that  $\hat{k}_x = 0, \hat{k}_y = \sin \epsilon = 0.3978, \hat{k}_z = \cos \epsilon = 0.9175$ .

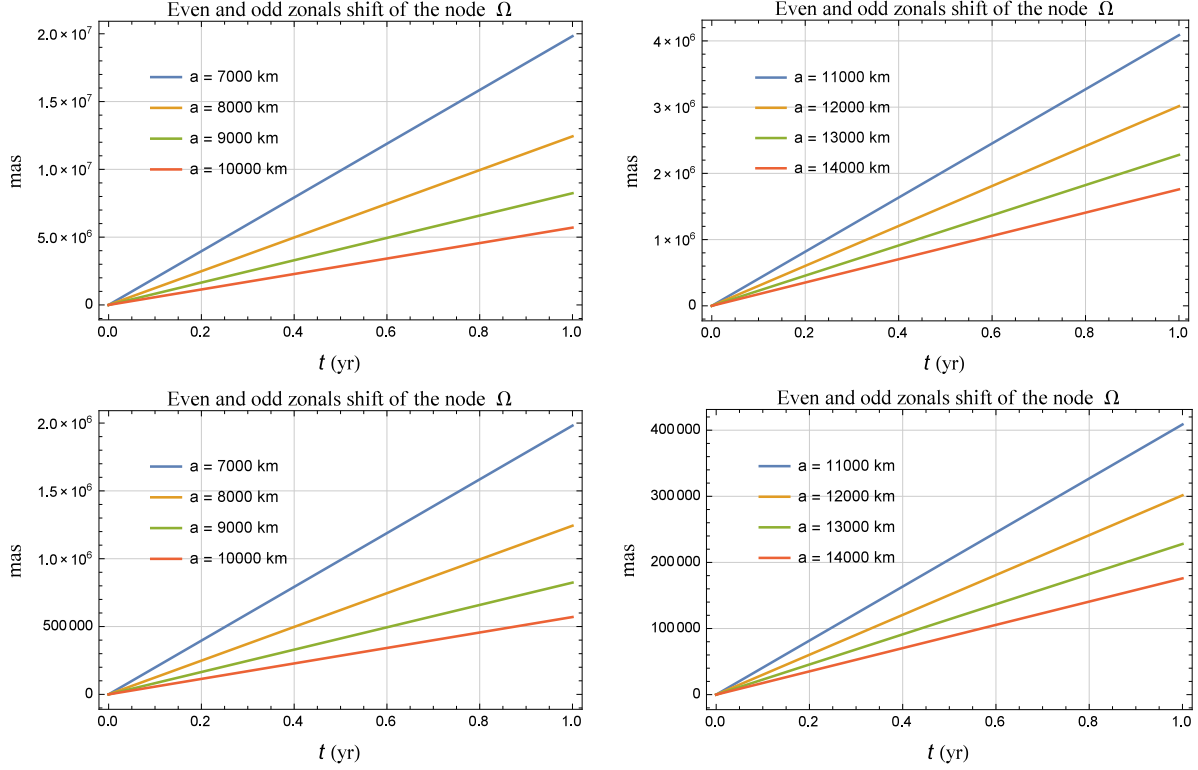


Fig. 5.— Upper row: nominal annual shifts of the satellite’s node  $\Omega$  obtained for different values of  $a$  by subtracting two time series produced by numerically integrating the equations of motion in rectangular Cartesian coordinates with and without the classical accelerations due to the first five even zonal harmonics  $J_2, J_3, J_4, J_5, J_6$  of the geopotential. Both the runs shared the same initial conditions characterized, among other things, by  $e = 0, \Omega = I = 90 \pm 0.1$  deg. Lower row: same as in the upper row, apart from an offset of  $0.01$  deg from the ideal condition  $I = \Omega = 90$  deg. The largest contribution is due to  $J_2$ , whose present-day uncertainty may be as large as  $\lesssim 2 \times 10^{-10}$  if evaluated conservatively; the statistical, formal errors  $\sigma_{\bar{C}_{2,0}}$  released in the global gravity field models produced from the GRACE/GOCE data by several institutions around the world are even  $\simeq 1 - 3$  orders of magnitude smaller. In both cases, a reference frame with the mean ecliptic at the epoch J2000.0 was used as reference  $\{x, y\}$  plane so that  $\hat{k}_x = 0, \hat{k}_y = \sin \epsilon = 0.3978, \hat{k}_z = \cos \epsilon = 0.9175$ .

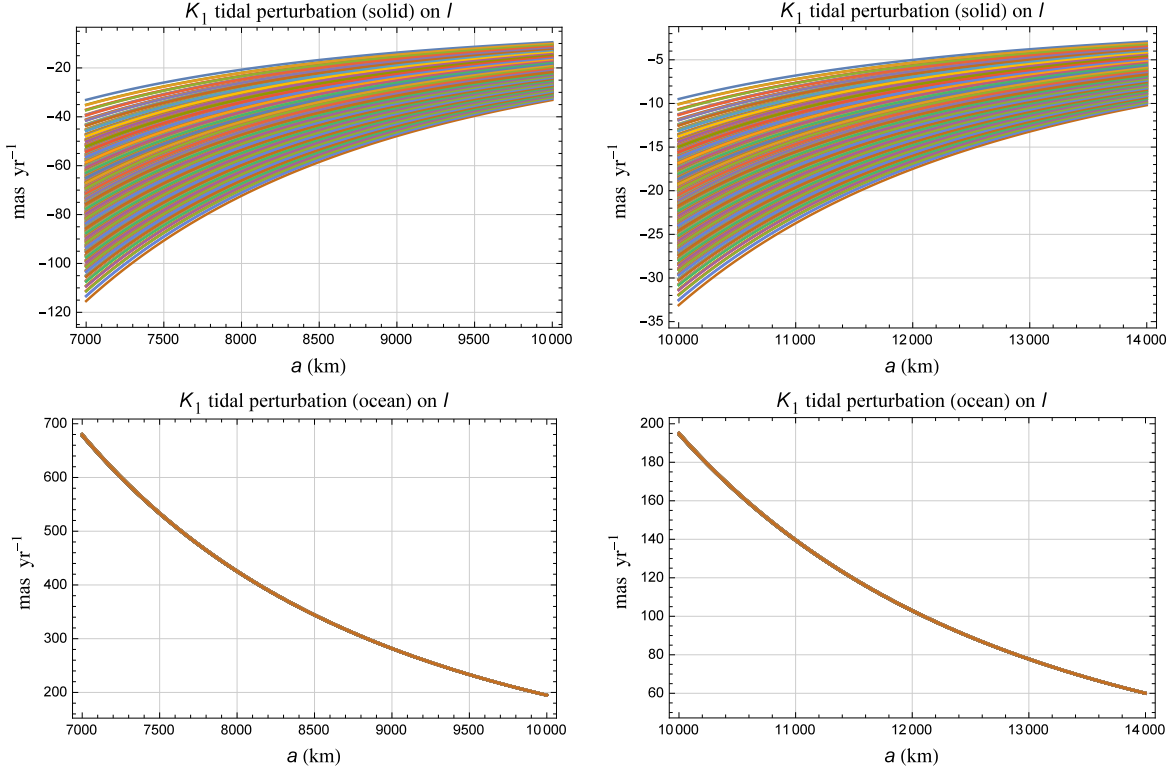


Fig. 6.— Nominal perturbations due to the solid (upper row) and ocean (lower row) component of the  $\ell = 2$ ,  $m = 1$ ,  $p = 1$ ,  $q = 0$  constituent of the  $K_1$  tide on the satellite’s inclination  $I$  as functions of  $a$ , as per Equations (30) to (36). In all the panels, each curve corresponds to a pair of values of  $I$ ,  $\Omega$  within the ranges  $I = \Omega = 90 \pm 0.05$  deg. The current level of uncertainty in the Love number  $k_{2,1,K_1}$  is of the order of  $\approx 10^{-3}$  or, perhaps, one order of magnitude better (Jagoda et al. 2018). According to the past EMG96 model (Lemoine et al. 1998),  $C_{2,1,K_1}^+$  was known with a relative accuracy of  $4 \times 10^{-2}$ . However, by calculating mean and standard deviation of the values computed at <https://bowie.gsfc.nasa.gov/ggfc/tides/harmonics.html> from the models TPXO.6.2 (Egbert & Erofeeva 2002), GOT99 (Ray 1999) and FES2004 (Lyard et al. 2006), a relative uncertainty of  $1.8 \times 10^{-3}$  is inferred.

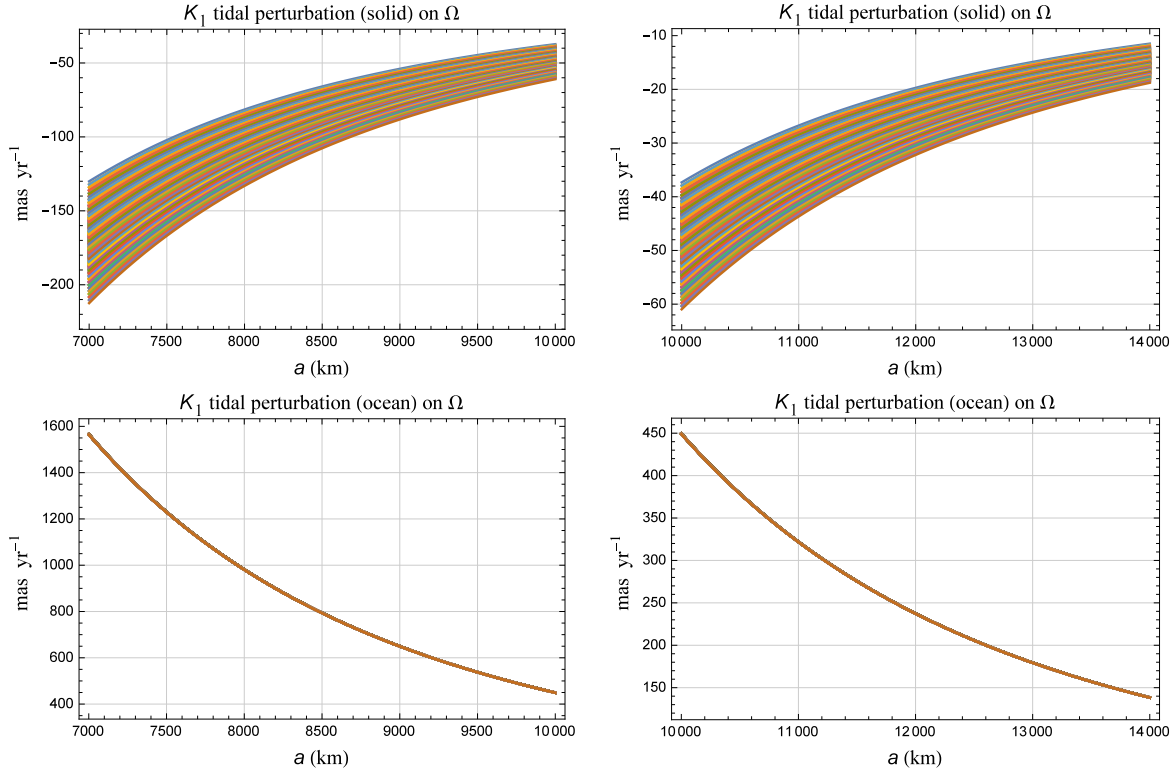


Fig. 7.— Nominal perturbations due to the solid (upper row) and ocean (lower row) component of the  $\ell = 2$ ,  $m = 1$ ,  $p = 1$ ,  $q = 0$  constituent of the  $K_1$  tide on the satellite's node  $\Omega$  as functions of  $a$ , as per Equations (31) to (37). In all the panels, each curve corresponds to a pair of values of  $I$ ,  $\Omega$  within the ranges  $I = \Omega = 90 \pm 0.05$  deg. The current level of uncertainty in the Love number  $k_{2,1,K_1}$  is of the order of  $\approx 10^{-3}$  or, perhaps, one order of magnitude better (Jagoda et al. 2018). According to the past EMG96 model (Lemoine et al. 1998),  $C_{2,1,K_1}^+$  was known with a relative accuracy of  $4 \times 10^{-2}$ . However, by calculating mean and standard deviation of the values computed at <https://bowie.gsfc.nasa.gov/ggfc/tides/harmonics.html> from the models TPXO.6.2 (Egbert & Erofeeva 2002), GOT99 (Ray 1999) and FES2004 (Lyard et al. 2006), a relative uncertainty of  $1.8 \times 10^{-3}$  is inferred.

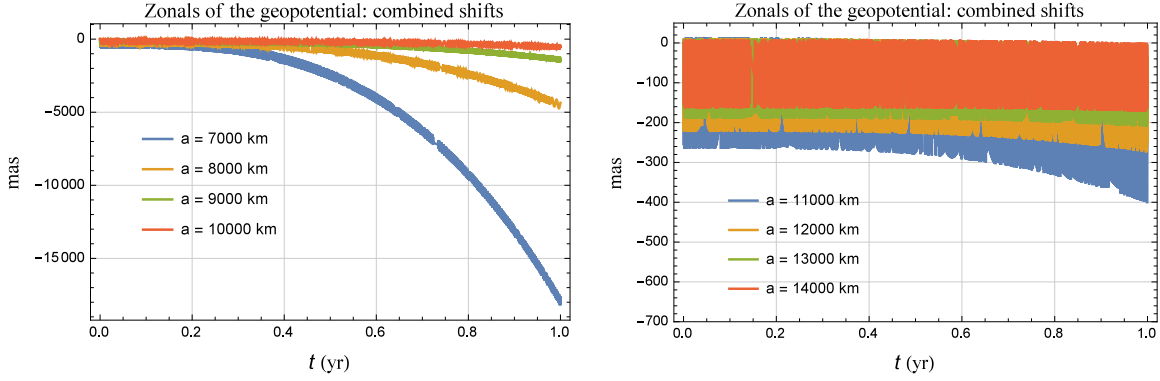


Fig. 8.— Numerically generated nominal amplitudes of the precessions of the satellite’s inclination and node induced by the first five even zonal harmonics  $J_2, J_3, J_4, J_5, J_6$  of the geopotential linearly combined according to Equations (40) to (41). They were obtained, for different values of  $a$ , by subtracting two time series for the combination of Equations (40) to (41) produced by numerically integrating the equations of motion in rectangular Cartesian coordinates with and without the classical accelerations due to  $J_\ell$ ,  $\ell = 2, 3, 4, 5, 6$ . Both the runs shared the same initial conditions characterized, among other things, by  $e = 0, \Omega = I = 90 \pm 0.1$  deg. The largest contribution is due to  $J_2$ , whose present-day uncertainty may be as large as  $\lesssim 2 \times 10^{-10}$  if evaluated conservatively; the statistical, formal errors  $\sigma_{\bar{C}_{2,0}}$  released in the global gravity field models produced from the GRACE/GOCE data by several institutions around the world are even  $\simeq 1 - 3$  orders of magnitude smaller. In both cases, a reference frame with the mean ecliptic at the epoch J2000.0 was used as reference  $\{x, y\}$  plane so that  $\hat{k}_x = 0$ ,  $\hat{k}_y = \sin \epsilon = 0.3978$ ,  $\hat{k}_z = \cos \epsilon = 0.9175$ .

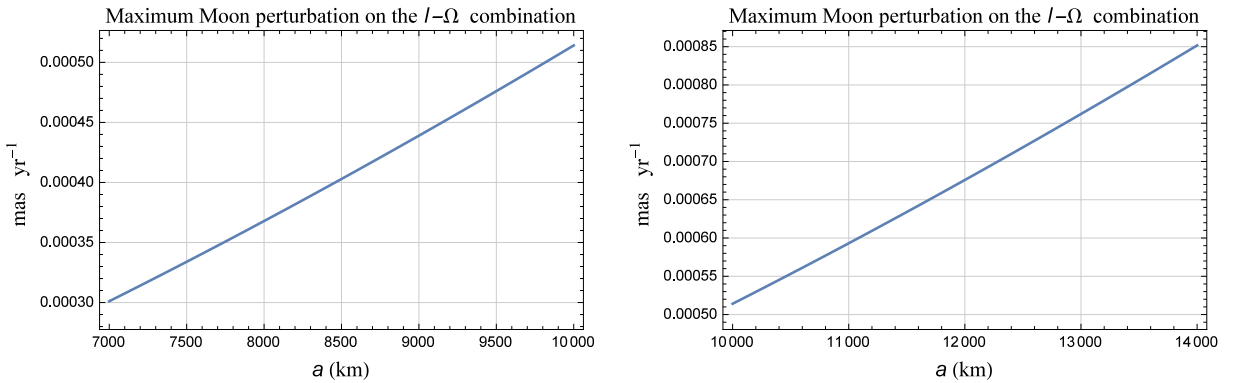


Fig. 9.— Maximum value, in  $\text{mas yr}^{-1}$ , of the mismodelled part of the 3rd-body precessions of  $I, \Omega$  due to the Moon combined with Equations (40) to (41) as a function of the satellite’s semimajor axis  $a$ ; Equation (50) was used. We assumed a relative uncertainty in  $\mu_{\mathcal{Q}}$  of  $2 \times 10^{-8}$ , as per the Object Data Page of the Moon provided by the JPL HORIZONS Web interface, revised on 2013.

## REFERENCES

- Abdel-Aziz Y. A., Khalil K. I., 2014, *Res. Astron. Astrophys.*, 14, 589
- Bertotti B., Farinella P., Vokrouhlický D., 2003, *Physics of the Solar System*. Kluwer, Dordrecht
- Brumberg V. A., Kopeikin S. M., 1989, *Nuovo Cimento B*, 103, 63
- de Sitter W., 1916, *Mon. Not. Roy. Astron. Soc.*, 77, 155
- Eanes R., Schuler A., 1999, in *EGS 24th General Assembly*, Hague, Netherlands
- Egbert G. D., Erofeeva S. Y., 2002, *J. Atmos. Oceanic Tech.*, 19, 183
- Everitt C. W. F. et al., 2011, *Phys. Rev. Lett.*, 106, 221101
- Everitt C. W. F. et al., 2015, *Classical Quant. Grav.*, 32, 224001
- Felsentreger T. L., Marsh J. G., Agreen R. W., 1976, *J. Geophys. Res.*, 81, 2557
- Ferraz Mello S., 1972, *Celest. Mech. Dyn. Astr.*, 5, 80
- Fokker A. D., 1920, *Versl. Kon. Ak. Wet.*, 29, 611
- Hofmann F., Müller J., 2018, *Classical Quant. Grav.*, 35, 035015
- Iorio L., 2001, *Celest. Mech. Dyn. Astr.*, 79, 201
- Iorio L., 2011, *Phys. Rev. D*, 84, 124001
- Iorio L., 2012a, *J. High Energy Phys.*, 5, 73
- Iorio L., 2012b, *Celest. Mech. Dyn. Astr.*, 112, 117
- Iorio L., 2018, *ArXiv e-prints*
- Jagoda M., Rutkowska M., Kraszewska K., Suchocki C., 2018, *Stud. Geophys. Geod.*, at press, 1
- Kahn R., 2007, *The Gravity Probe B Experiment. “Testing Einstein’s Universe”. Post Flight Analysis-Final Report*. Stanford University
- Lemoine F. G. et al., 1998, *The Development of the Joint NASA GSFC and the National Imagery and Mapping Agency (NIMA) Geopotential Model EGM96*. NASA/TP-1998-206861. Goddard Space Flight Center, Greenbelt
- Lense J., Thirring H., 1918, *Physikalische Zeitschrift*, 19, 156

- Lerch F. J. et al., 1992, Geopotential models of the Earth from satellite tracking, altimeter and surface gravity observations: GEM-T3 and GEM-T3S. NASA Technical Memorandum 104555. Goddard Space Flight Center, Greenbelt
- Lhotka C., Celletti A., Gałęs C., 2016, Mon. Not. Roy. Astron. Soc., 460, 802
- Lucchesi D. M., 2001, Planet. Space Sci., 49, 447
- Lucchesi D. M., 2002, Planet. Space Sci., 50, 1067
- Lyard F., Lefevre F., Letellier T., Francis O., 2006, Oc. Dyn., 56, 394
- Mayer-Gürr T., Savcenko R., Bosch W., Daras I., Flechtner F., Dahle C., 2012, J. Geodyn., 59, 28
- Milani A., Nobili A., Farinella P., 1987, Non-gravitational perturbations and satellite geodesy. Adam Hilger, Bristol
- Murray C. D., Dermott S. F., 2000, Solar System Dynamics. Cambridge University Press
- Petit G., Luzum B., et al., 2010, IERS Technical Note, 36, 1
- Pitjeva E. V., 2015, J. Phys. Chem. Ref. Data, 44, 031210
- Pugh G., 1959, Proposal for a Satellite Test of the Coriolis Prediction of General Relativity. Research Memorandum 11, Weapons Systems Evaluation Group, The Pentagon, Washington D.C.
- Ray R., 1999, A global ocean tide model from topex/poseidon altimetry: Got99. NASA Technical Memorandum NASA/TM209478, Goddard Space Flight Center, Greenbelt, USA
- Renzetti G., 2013, J. Astrophys. Astron., 34, 341
- Renzetti G., 2014, Astrophys. Space Sci., 352, 493
- Savcenko R., Bosch W., 2012, EOT11a Empirical ocean tide model from multi-mission satellite altimetry. Deutsches Geodätisches Forschungsinstitut, München
- Schaechter D., Breakwell J. V., van Patten R. A., Everitt C. W. F., 1977, J. Spacecraft Rockets, 14, 474
- Schaechter D., Breakwell J. V., van Patten R. A., Everitt F. W., 1976, J. Astronaut. Sci., 24, 137
- Schiff L., 1960, Physical Review Letters, 4, 215
- Schouten W. J. A., 1918, Versl. Kon. Ak. Wet., 27, 214
- Sehna L., 1981, Celest. Mech. Dyn. Astr., 25, 169



- Thorne K. S., 1983, in Quantum Optics, Experimental Gravity, and Measurement Theory, Meystre P., Scully M. O., eds., Springer, Boston, MA, pp. 325–346
- van Patten R. A., Breakwell J. V., Schaechter D., Everitt C. W. F., 1978, *Acta Astronaut.*, 5, 77
- van Patten R. A., Everitt C. W. F., 1976a, *Celest. Mech. Dyn. Astr.*, 13, 429
- van Patten R. A., Everitt C. W. F., 1976b, *Phys. Rev. Lett.*, 36, 629
- Wagner C. A., McAdoo D. C., 2012, *J. Geodesy*, 86, 99